Electromagnetic Scattering From a Dielectric Cylinder Buried Beneath a Slightly Rough Surface

Daniel E. Lawrence, *Student Member, IEEE,* and Kamal Sarabandi, *Fellow, IEEE*

***Abstract*—An analytical solution is presented for the electromagnetic scattering from a dielectric circular cylinder embedded in a dielectric half-space with a slightly rough interface. The solution utilizes the spectral (plane-wave) representation of the fields and accounts for all the multiple interactions between the rough interface and the buried cylinder. First-order coefficients from the small perturbation method are used for computation of the scattered fields from the rough surface. The derivation includes both TM and TE polarizations and can be easily extended for other cylindrical buried objects (e.g., cylindrical shell, metallic cylinder). Several scattering scenarios are examined utilizing the new solution for a dielectric cylinder beneath a flat, sinusoidal, and arbitrary rough surface profile. Results indicate that the scattering pattern of a buried object below a slightly rough surface differs from the flat surface case only when the surface roughness spectrum contains a limited range of spatial frequencies. Furthermore, the illuminated area of the incident wave is seen to be a critical factor in the visibility of a buried object below a rough surface.**

***Index Terms*—Buried objects, ground penetrating radar, rough surfaces, scattering.**

I. Introduction

OVER the past few decades, a significant amount of research effort has been spent toward developing a viable buried object detection scheme. The results of such research can be applied to buried landmines, pipes, conduits, and other buried objects of interest. There are many difficulties associated with detecting objects beneath the ground due to the existence of clutter and low RF signal penetration into moist soil. Recently, the authors proposed an acousto–electromagnetic approach to enhance buried object detection by observing the scattered electromagnetic Doppler spectrum from an object vibrated at resonance [1] and [2]. In addition to the object vibration, the incident and scattered acoustic waves will perturb the interface above the buried object. In a similar detection technique proposed by Scott [3], a Doppler radar is used in conjuction with elastic waves in the ground to detect buried objects by anomolies found in the surface vibration. In both of these techniques, it is important to characterize the relative backscatter from the acoustic-induced surface roughness and buried object, including the direct backscatter and all multiple interactions between the object and rough surface. The interface may also be naturally rough. Accordingly, this paper will present an analytical solution for a two-dimensional (2-D) scattering problem involving a buried dielectric circular cylinder below a slightly rough surface.

The analysis of a buried cylinder below a flat surface has been done analytically by D'Yakonov [4], and subsequently has been examined by Howard [5] and Ogunade [6], where the solution was obtained by the eigenfunction expansion of the total fields. A number of other analytical studies involving the scattering from buried objects below a flat interface have also been done [7]–[12]. Butler [13] and Xu [14] have solved the problem of a buried conducting cylinder of arbitrary geometry below a flat surface using the method of moments (MoM). In each of these works, the assumption of a flat surface was critical for mathematical and computational tractability. For practical considerations, however, it is necessary to understand the effect of a rough surface on the scattering from buried objects. Generally, ground penetrating radar (GPR) systems use oblique incidence to direct the strong specular reflection away from the backscatter receiver. While this helps isolate the return from the buried object, rough surface scattering can still interfere with the target return. Only recently has there been any consideration of a target beneath a rough surface. Cottis and Kanellopoulos treat the scattering from a circular cylinder buried below a sinusoidal interface, using an integral equation combined with the extended boundary condition approach [15] and [16]. Several other numerical studies involving a buried object below a rough surface have also been done recently [17]–[21].

Analytical scattering solutions such as the small perturbation method (SPM) and Kirchhoff approximation are widely known and used to study the scattering from slightly-rough surfaces [22]–[24]. To date, the interaction of a buried object with a rough surface has not been explored analytically. Analytical solutions, unlike numerical techniques, are unfortunately limited to canonical geometries or small perturbations from a canonical geometry. Nevertheless, analytical solutions are valuable in that they do not require a discretization of the geometry and can provide a benchmark for comparison with numerical solutions. Furthermore, fundamental insight into the scattering mechanisms of a problem can be gained from an analytical approach. In this paper, an analytical solution for a buried circular cylinder beneath a slightly rough surface [with arbitrary one-dimensional (1-D) surface profile] is derived. The

Manuscript received April 19, 2001; revised December 15, 2001. This work was supported by DoD HPCMO under a Subcontract from HPT, Inc.

The authors are with the Radiation Laboratory, Department of Electrical Engineering and Computer Science, University of Michigan, Ann Arbor, MI 48109-2122 USA.

Digital Object Identifier 10.1109/TAP.2002.802160

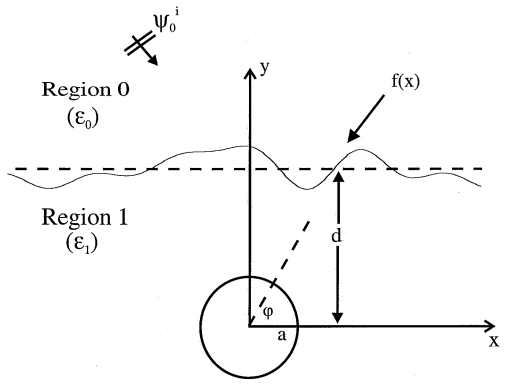

Fig. 1. Geometry of scattering problem.

solution is obtained by employing the spectral, plane-wave representation of the fields and adding the successive reflections from the rough half-space boundary and the scattered fields from the cylinder. All of the multiple interactions are accounted for in this solution. First-order reflection and transmission coefficients from the SPM are used for the rough-surface scattering. As a result, the ultimate accuracy of the analytical approach presented here is limited by the accuracy of the SPM solution. Details of the analytical development are presented in Section II followed by several illustrative examples in Section III utilizing the new solution.

II. Analytical Development

A. Initial Reflected and Transmitted Fields

Consider a plane-wave incident upon a slightly-rough surface (1-D roughness) with a dielectric cylinder of radius a buried at a depth d beneath the surface. The geometry of the scattering scenario is shown in Fig. 1. The surface of the half-space has a 1-D profile given by the function $f(x)$. The Fourier transform of this function is needed in the development that follows and is defined by

$$F(k_x) = \frac{1}{2\pi}\int_{-\infty}^{\infty} f(x)e^{jk_x x}\,dx. \tag{1}$$

The method used in this section to solve for the scattered field in Region 1 will employ the spectral representation of the fields. Since analytical solutions for the scattering of a plane wave from a slightly rough interface and the scattering of a plane wave from a cylinder are known, the solution will be formed by adding the successive scattered fields from the rough interface and the cylinder. Both TE and TM polarizations will be treated simultaneously by using only general expressions for the reflected, transmitted, and scattered fields. In this paper, we define TE and TM to be transverse to the axis of the cylinder, the z axis. Note that this is the usual convention for cylinder scattering problems, but is opposite the usual convention for rough surface scattering. The incident field is expressed

$$\psi_0^i = e^{-j\left(k_x^i x - k_{0y}^i y\right)} \tag{2}$$

where ψ is a scalar quantity equal to E_z for the TM case or H_z for the TE case. Using the SPM solution, the reflected and transmitted fields at the interface with no cylinder present can be obtained. Complete expressions for the relevant coefficients of the reflected and transmitted fields are provided in the Appendix. To first-order, the field initially reflected from the boundary can be written

$$\begin{aligned}\psi_0^r = {} & R_{01}(k_x^i)e^{j2k_{0y}^i d}e^{-j\left(k_x^i x + k_{0y}^i y\right)} \\ & + \int_{-\infty}^{\infty} r_{01}(k_x)e^{j\left(k_{0y}^i + k_{0y}\right)d}e^{-j(k_x x + k_{0y} y)}dk_x\end{aligned} \tag{3}$$

where $k_{0y} = \sqrt{k_0^2 - k_x^2}$. $R_{01}(k_x^i)$ and $r_{01}(k_x)$ are the coefficients for the unperturbed and perturbed components of the reflected field, respectively. Again to first-order, the field transmitted into Region 1 is

$$\begin{aligned}\psi_1^t = {} & T_{01}(k_x^i)e^{j\left(k_{0y}^i - k_{1y}^i\right)d}e^{-j\left(k_x^i x - k_{1y}^i y\right)} \\ & + \int_{-\infty}^{\infty} \tau_{01}(k_x)e^{j(k_{0y} - k_{1y})d}e^{-j(k_x x - k_{1y} y)}dk_x \\ = {} & \int_{-\infty}^{\infty}\left[T_{01}(k_x)\delta(k_x - k_x^i) + \tau_{01}(k_x)\right] \\ & \times e^{j(k_{0y} - k_{1y})d}e^{-j(k_x x - k_{1y} y)}dk_x\end{aligned} \tag{4}$$

where $k_{1y} = \sqrt{k_1^2 - k_x^2}$. $T_{01}(k_x^i)$ and $\tau_{01}(k_x)$ are the coefficients for the unperturbed and perturbed components of the transmitted field, respectively. The spectral representation in (4) shows that the transmitted field is composed of a spectrum of plane waves traveling in the $-y$-direction, specifically determined by k_x, and weighted accordingly.

B. Scattered Fields in Region 1

The initial scattered field from the cylinder can be found by treating each plane wave of the transmitted field in (4) as being incident upon the buried cylinder. The eigenfunction solution for the scattering of a plane wave from a cylinder in a homogeneous medium is well known [25]. For a single, unity amplitude plane wave incident at an angle ϕ_i the scattered field is

$$\psi_1 = \sum_{n=-\infty}^{\infty} j^{-n}A_n H_n^{(2)}(k_1\rho)e^{jn(\phi - \phi_i)} \tag{5}$$

where A_n are mode coefficients for the scattered field. Depending on the polarization, these coefficients are

$$A_n = \frac{\frac{\eta_1}{\eta_2}J_n(k_1 a)J_n'(k_2 a) - J_n'(k_1 a)J_n(k_2 a)}{J_n(k_2 a)H_n^{(2)'}(k_1 a) - \frac{\eta_1}{\eta_2}J_n'(k_2 a)H_n^{(2)}(k_1 a)} \text{ (TM Case)}$$

$$A_n = \frac{\frac{\eta_2}{\eta_1}J_n(k_1 a)J_n'(k_2 a) - J_n'(k_1 a)J_n(k_2 a)}{J_n(k_2 a)H_n^{(2)'}(k_1 a) - \frac{\eta_2}{\eta_1}J_n'(k_2 a)H_n^{(2)}(k_1 a)} \text{ (TE Case).}$$

For this paper, only a solid dielectric cylinder is considered, but in general, the mode coefficients for other cylindrical objects of interest such as a metallic cylinder or dielectric cylindrical shell could be inserted for A_n. With ψ_1^t incident upon the cylinder, the scattered field can easily be written to account for the spectrum of incident plane waves by integration over k_x. Integrating the eigenfunction solution in (5) over k_x and using the appropriate weighting from (4), the initial scattered field becomes

$$\begin{aligned}\psi_1^{(1)} = {} & \int_{-\infty}^{\infty}\sum_{n=-\infty}^{\infty} j^{-n}A_n H_n^{(2)}(k_1\rho)e^{jn\left[\phi - \tan^{-1}(-k_{1y}/k_x)\right]} \\ & \times\left[T_{01}\delta(k_x - k_x^i) + \tau_{01}(k_x)\right]e^{j(k_{0y} - k_{1y})d}dk_x \\ = {} & \sum_{n=-\infty}^{\infty} j^{-n}A_n H_n^{(2)}(k_1\rho)e^{jn\phi}\left[C_n^{(1)} + \Delta D_n^{(1)}\right]\end{aligned} \tag{6}$$

where

$$C_n^{(1)} = T_{01}(k_x^i) e^{j\left(k_{0y}^i - k_{1y}^i\right)d} e^{-jn\tan^{-1}\left(-k_{1y}^i/k_x^i\right)}$$
$$\Delta D_n^{(1)} = \int_{-\infty}^{\infty} \tau_{01}(k_x) e^{j\left(k_{0y}^i - k_{1y}\right)d} e^{-jn\tan^{-1}(-k_{1y}/k_x)} dk_x.$$

Δ here denotes a small quantity since $\tau_{01}(k_x)$ is directly proportional to the small-surface roughness. The expression in (6) is the scattered field resulting from the first interaction with the buried cylinder. Subsequent calculations will add the contribution from the successive reflections from the boundary and scattering from the cylinder. Using the integral expansion of $H_n^{(2)}(k_1\rho)e^{jn\phi}$ [26], (6) can be expanded into its spectral representation as

$$\psi_1^{(1)} = \frac{1}{\pi}\int_{-\infty}^{\infty} \frac{e^{-j(k_x x + k_{1y} y)}}{k_{1y}} \sum_{n=-\infty}^{\infty} A_n \times \left[C_n^{(1)} + \Delta D_n^{(1)}\right] e^{jn\tan^{-1}(k_{1y}/k_x)} dk_x. \quad (7)$$

This representation is seen to be a linear combination of plane waves propagating in the $+y$-direction, specifically determined by k_x and incident upon the rough surface from below. Hence, the reflection coefficients from the SPM solution can be included in the integral, and the downward traveling field reflected from the perturbed boundary becomes

$$\tilde{\psi}_1^{(1)} = \frac{1}{\pi}\int_{k_x} \frac{1}{k_{1y}} \sum_{n=-\infty}^{\infty} A_n \left[C_n^{(1)} + \Delta D_n^{(1)}\right] e^{jn\tan^{-1}(k_{1y}/k_{1x})} \times \left[R_{10}(k_x) e^{-2jk_{1y}d} e^{-j(k_x x - k_{1y} y)} + \int_{k_x'} r_{10}(k_x, k_x') e^{-j\left(k_{1y} + k_{1y}'\right)d} e^{-j\left(k_x' x - k_{1y}' y\right)} dk_x'\right] \times dk_x. \quad (8)$$

Reflection coefficients with subscript "10" are used since the fields are incident from Region 1. The superposition of downward traveling plane waves described by (8) now become incident upon the cylinder. Once again, the known eigenfunction solution for the scattered field from a cylinder with plane wave incidence is employed. Integrating the eigenfunction solution in (5) over k_x and using the appropriate weighting from (8), the second scattered field from the cylinder can be written

$$\psi_1^{(2)} = \sum_{n=-\infty}^{\infty} j^{-n} A_n H_n^{(2)}(k_1\rho) e^{jn\phi} \times \left[\frac{1}{\pi}\sum_{m=-\infty}^{\infty} A_m \left(C_m^{(1)} + \Delta D_m^{(1)}\right)\left(I_{m,n}^u + \Delta I_{m,n}^p\right)\right] \quad (9)$$

where

$$I_{m,n}^u = \int_{k_x} \frac{1}{k_{1y}} R_{10}(k_x) e^{-2jk_{1y}d} e^{jm\tan^{-1}(k_{1y}/k_x)} \times e^{-jn\tan^{-1}(-k_{1y}/k_x)} dk_x$$
$$\Delta I_{m,n}^p = \int_{k_x}\int_{k_x'} \frac{1}{k_{1y}} r_{10}(k_x, k_x') e^{-j\left(k_{1y} + k_{1y}'\right)d} \times e^{jm\tan^{-1}(k_{1y}/k_x)} e^{-jn\tan^{-1}\left(-k_{1y}'/k_x'\right)} dk_x' dk_x.$$

Both $\Delta D_n^{(1)}$ and $\Delta I_{m,n}^p$ are small quantities containing the perturbation parameter Δ. By keeping only first-order terms in Δ we can rewrite (9)

$$\psi_1^{(2)} = \sum_{n=-\infty}^{\infty} j^{-n} A_n H_n^{(2)}(k_1\rho) e^{jn\phi} \left[C_n^{(2)} + \Delta D_n^{(2)}\right] \quad (10)$$

where

$$C_n^{(2)} = \frac{1}{\pi}\sum_{m=-\infty}^{\infty} A_m C_m^{(1)} I_{m,n}^u$$
$$\Delta D_n^{(2)} = \frac{1}{\pi}\sum_{m=-\infty}^{\infty} A_m \left(C_m^{(1)} \Delta I_{m,n}^p + \Delta D_m^{(1)} I_{m,n}^u\right).$$

Equation (10) represents the second scattered field from the buried cylinder. In general, the qth scattered field can be written

$$\psi_1^{(q)} = \sum_{n=-\infty}^{\infty} j^{-n} A_n H_n^{(2)}(k_1\rho) e^{jn\phi} \left[C_n^{(q)} + \Delta D_n^{(q)}\right] \quad (11)$$

where

$$C_n^{(q)} = \frac{1}{\pi}\sum_{m=-\infty}^{\infty} A_m C_m^{(q-1)} I_{m,n}^u \quad (12)$$
$$\Delta D_n^{(q)} = \frac{1}{\pi}\sum_{m=-\infty}^{\infty} A_m \times \left(C_m^{(q-1)} \Delta I_{m,n}^p + \Delta D_m^{(q-1)} I_{m,n}^u\right). \quad (13)$$

Note from (12) and (13), that the qth coefficients are found in terms of the $(q-1)$th coefficients, indicating the recursive nature of this solution. The total scattered field in Region 1 can be obtained by adding each successive scattered field. That is

$$\psi_1 = \sum_{q=1}^{\infty} \psi_1^{(q)} \quad (14)$$
$$= \sum_{q=1}^{\infty}\sum_{n=-\infty}^{\infty} j^{-n} A_n H_n^{(2)}(k_1\rho) e^{jn\phi} \times \left[C_n^{(q)} + \Delta D_n^{(q)}\right] \quad (15)$$
$$= \sum_{n=-\infty}^{\infty} j^{-n} A_n H_n^{(2)}(k_1\rho) e^{jn\phi} \times \left[\mathcal{C}_n + \Delta\mathcal{D}_n\right] \quad (16)$$

where

$$\mathcal{C}_n = \sum_{q=1}^{\infty} C_n^{(q)} \text{ and } \Delta\mathcal{D}_n = \sum_{q=1}^{\infty} \Delta D_n^{(q)}. \quad (17)$$

One way to calculate the coefficients $\mathcal{C}_n$ and $\Delta\mathcal{D}_n$, is to begin with the known coefficients from the first interaction, $C_n^{(1)}$ and $D_n^{(1)}$, use the recursive (12) and (13), and add each successive

term until the result converges. An alternative method for obtaining the coefficients, which includes *all* the multiple interactions, can be seen by rewriting $\mathcal{C}_n$ in (17)

$$\mathcal{C}_n = C_n^{(1)} + \sum_{q=1}^{\infty} C_n^{(q+1)} \tag{18}$$

$$= C_n^{(1)} + \sum_{q=1}^{\infty} \frac{1}{\pi} \sum_{m=-\infty}^{\infty} A_m C_m^{(q)} I_{m,n}^u \tag{19}$$

$$= C_n^{(1)} + \frac{1}{\pi} \sum_{m=-\infty}^{\infty} A_m \mathcal{C}_m I_{m,n}^u. \tag{20}$$

Equation (20) represents and infinite set of equations to solve for the unknown coefficients, $\mathcal{C}_n$. For computational purposes, a truncation in n and m can be chosen to conveniently solve the system using matrix techniques. Similarly, $\Delta\mathcal{D}_n$ can be rewritten

$$\Delta\mathcal{D}_n = \Delta D_n^{(1)} + \sum_{q=1}^{\infty} \Delta D_n^{(q+1)} \tag{21}$$

$$= \Delta D_n^{(1)} + \sum_{q=1}^{\infty} \frac{1}{\pi} \sum_{m=-\infty}^{\infty} A_m \times \left(C_m^{(q)} \Delta I_{m,n}^p + \Delta D_m^{(q)} I_{m,n}^u \right) \tag{22}$$

$$= \Delta D_n^{(1)} + \frac{1}{\pi} \sum_{m=-\infty}^{\infty} A_m \times \left(\mathcal{C}_m \Delta I_{m,n}^p + \Delta\mathcal{D}_m I_{m,n}^u \right). \tag{23}$$

Once again, an infinite set of equations is obtained. Note that the coefficients $\mathcal{C}_n$, found from (20) are used here to solve for $\Delta\mathcal{D}_n$. It is worth mentioning again, that although a truncation in n and m is required to solve (20) and (23), the resulting coefficients include all the multiple interactions between the rough surface and the buried cylinder.

C. Scattered Fields in Region 0

In order to compute the scattered field in Region 0, the scattered field in Region 1 is first expanded into spectral form. Using the integral expansion of $H_n^{(2)}(k_1\rho)e^{jn\phi}$, the scattered field of (16) becomes

$$\psi_1 = \frac{1}{\pi} \int_{k_x} \frac{1}{k_{1y}} e^{-j(k_x x + k_{1y} y)} \sum_{n=-\infty}^{\infty} A_n \times (C_n + \Delta D_n) e^{jn \tan^{-1}(k_{1y}/k_x)} dk_x. \tag{24}$$

The spectrum of upward traveling plane waves described by this equation are transmitted through the interface and scaled by the transmission coefficients to produce the scattered field in Region 0. Once the transmission coefficients are included, the scattered field in Region 0 can be expressed

$$\psi_0^s = \frac{1}{\pi} \sum_{n=-\infty}^{\infty} A_n (C_n + \Delta D_n) \left(I_n^{tu} + \Delta I_n^{tp} \right) \tag{25}$$

where

$$I_n^{tu} = \int_{k_x} \frac{1}{k_{1y}} T_{10}(k_x) e^{jn \tan^{-1}(k_{1y}/k_x)} \times e^{j(k_{0y} - k_{1y})d} e^{-j(k_x x + k_{0y} y)} dk_x$$

$$\Delta I_n^{tp} = \int_{k_x} \int_{k_x'} \frac{1}{k_{1y}} \tau_{10}(k_x, k_x') e^{jn \tan^{-1}(k_{1y}/k_x)} \times e^{j(k_{0y}' - k_{1y})d} e^{-j(k_x' x + k_{0y}' y)} dk_x' dk_x.$$

The total scattered field in Region 0 should include the initially reflected component from the rough interface, ψ_0^r, from (3). Accordingly, the total scattered field in Region 0 becomes

$$\psi_0 = \psi_0^r + \psi_0^s. \tag{26}$$

III. Simulations

Several cases are considered to demonstrate the general solution derived here and to illustrate the effect of the half-space and rough surface on the scattering pattern. In each case, the specular component of the initial reflected wave from the interface is not included. In order to calculate the far-field scattering pattern, the highly oscillatory integrals I_n^{tu} and ΔI_n^{tp} must be evaluated using the saddle point integration technique [27]. On the other hand, the integrals $I_{m,n}^u$ and $\Delta I_{m,n}^p$ can be evaluated directly provided the buried cylinder depth, d, is within a few wavelengths of the surface. Otherwise, asymptotic evaluation of these integrals is also required. The scattering scenarios to be presented include a dielectric cylinder buried beneath a: 1) flat surface; 2) sinusoidal surface; and 3) an arbitrary rough surface.

A. Flat Surface

When there is no surface variation, the scattering solution simplifies considerably. Terms containing the perturbation parameter Δ become zero, and the solution in (25) reduces to

$$\psi_0^s = \frac{1}{\pi} \sum_{n=-\infty}^{\infty} A_n C_n I_n^{tu}. \tag{27}$$

Although obtained by a different method, (27) is equivalent to the solution found in [9]. As an example, consider a dielectric cylinder $\epsilon = 2.25\epsilon_0$, with radius $a = 0.16\lambda_0$, buried below a flat surface at a depth $d = 1.3\lambda_0$. For a TE plane-wave incident at 30° from the y axis ($\phi_i = -60°$), Fig. 2 shows the bistatic scattering (far-field) pattern for different background permittivities. The far-field radar cross section (RCS) pattern shown in each of the plots is calculated by $\sigma = \lim_{\rho\to\infty} 2\pi\rho\,|\psi^s/\psi^i|^2$. In addition to reducing the magnitude of the scattered field, the presence of the interface and background permittivity also significantly affect the scattering pattern of the cylinder. Note that the null in the free space scattering pattern located at 40° in Fig. 2 moves outward, and ultimately disappears, as the background dielectric constant is increased.

B. Sinusoidal Surface

A great deal of insight into the scattering from objects buried below a rough interface can be obtained by looking at the scattering from a cylinder below a sinusoidal surface. Also, the

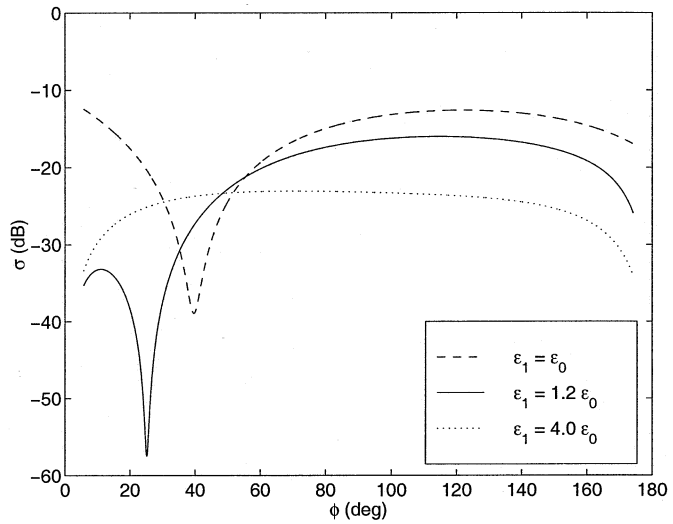

Fig. 2. Effect of ground permittivity on the scattering pattern of a dielectric cylinder, $\epsilon = 2.25\epsilon_0$, with radius $a = 0.16\lambda_0$, buried at depth $d = 1.3\lambda_0$, and $\phi_i = -60°$. (Unperturbed TE Case.)

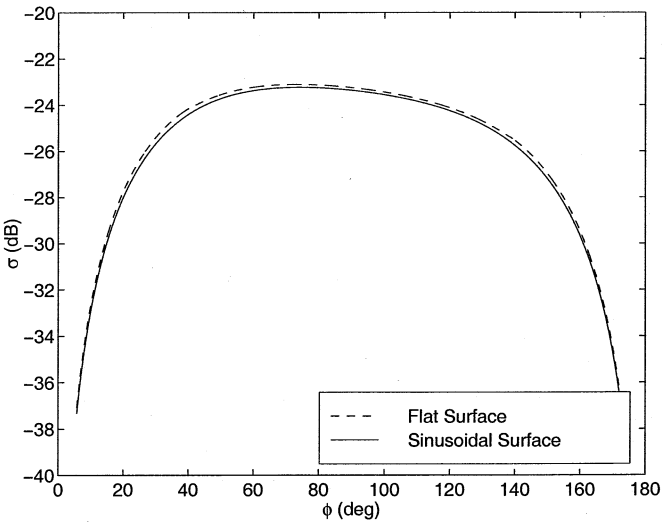

Fig. 3. Effect of sinusoidal surface roughness on the scattering pattern for $\lambda_s = 0.25\lambda_0$, $a = 0.16\lambda_0$.

expressions derived in this paper for a general rough surface simplify when the surface roughness is sinusoidal. Noting that the Fourier transform $F(k_x)$ of a sinusoidal surface variation (and hence the SPM coefficients) are composed of Dirac delta functions, the double integrals $\Delta I^p_{m,n}$ in (23) and ΔI^{tp}_n in (25) both reduce to single integrals in k_x. This simplification reduces both the complexity and computation time of the solution. Figs. 3–6 demonstrate the effect of a sinusoidal surface on the scattering of a TM plane wave incident at $\phi_i = -60°$ upon a buried dielectric cylinder, $a = 0.16\lambda_0$, $\epsilon = 2.25\epsilon_0$ and $\epsilon_1 = (4.0 - j0.01)\epsilon_0$, buried at a depth, $d = 1.3\lambda_0$, below the surface. Note that the discrete Floquet mode components of the initial reflected field are not shown. The surface variation function is

$$f(x) = 0.0064\lambda_0 \cos\left(\frac{2\pi}{\lambda_s}x\right) \tag{28}$$

where λ_s is the period of the surface which is varied from $0.25\lambda_0$ in Fig. 3 to $2.0\lambda_0$ in Fig. 6. As seen in Fig. 3, the scattering pattern for $\lambda_s = 0.25\lambda_0$ is almost identical to that of a flat surface. On the other hand, the scattering pattern is significantly changed for $\lambda_s = 0.4\lambda_0$ and $0.6\lambda_0$ as shown in Figs. 4 and 5. Note, however, for $\lambda_s = 2.0\lambda_0$ shown in Fig. 6 that the pattern once again approaches that of a flat surface. The conclusion here is that the scattering pattern of a buried object is only significantly affected by a limited range of (spatial) surface frequencies, and roughness outside this frequency range does not alter the scattering pattern. To determine whether this effect is dependent upon the size of the buried scatterer, simulations were repeated for a cylinder of radius $a = 1.0\lambda_0$ buried at depth $d = 1.3\lambda_0$. Results are shown in Figs. 7–10, and confirm that surface roughness outside a limited range of frequencies does not affect the scattering pattern of a larger buried object. Although not shown, this result holds for the TE case as well.

It is well known that the SPM scattering solution for random rough surfaces (without buried objects) is only valid when the surface correlation length is small [28]. Hence, a relevant ques-

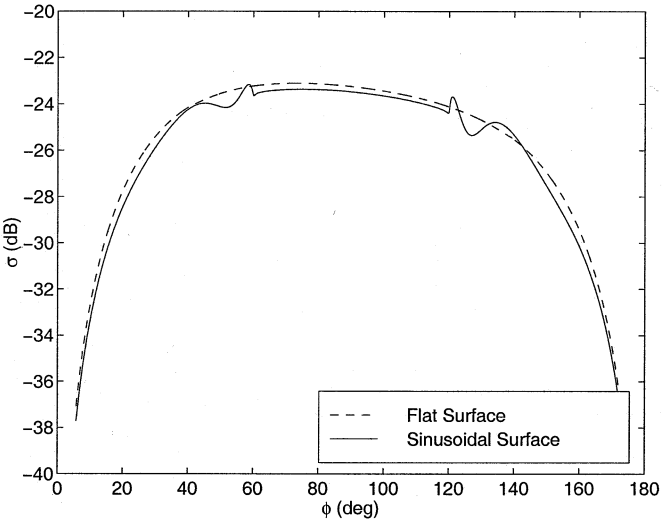

Fig. 4. Effect of sinusoidal surface roughness on the scattering pattern for $\lambda_s = 0.4\lambda_0$, $a = 0.16\lambda_0$.

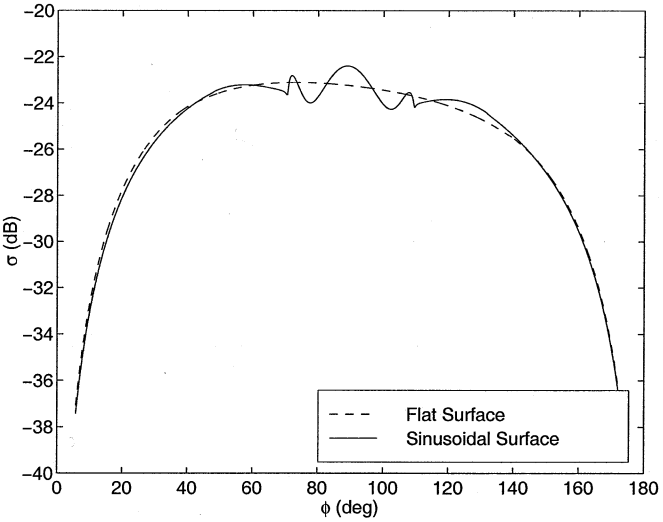

Fig. 5. Effect of sinusoidal surface roughness on the scattering pattern for $\lambda_s = 0.6\lambda_0$, $a = 0.16\lambda_0$.

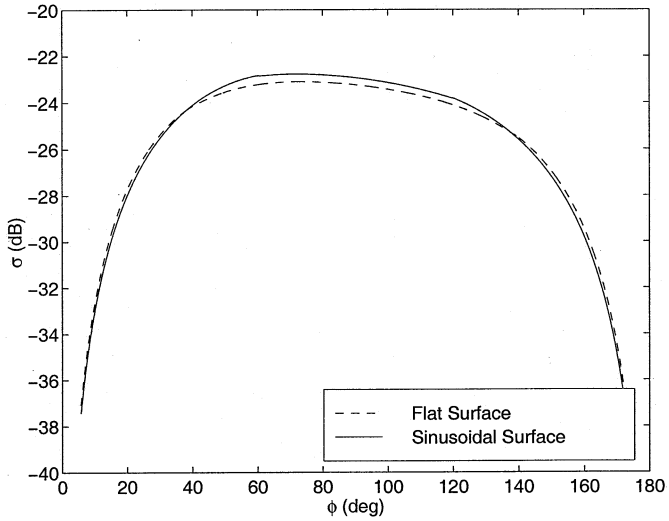

Fig. 6. Effect of sinusoidal surface roughness on the scattering pattern for $\lambda_s = 2.0\lambda_0$, $a = 0.16\lambda_0$.

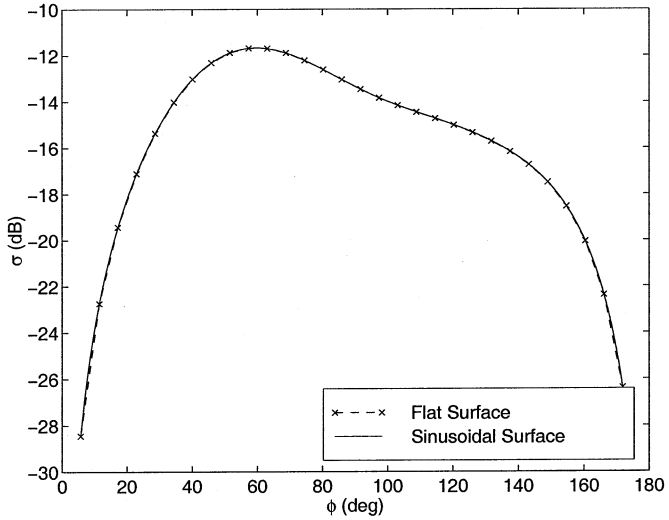

Fig. 7. Effect of sinusoidal surface roughness on the scattering pattern for $\lambda_s = 0.25\lambda_0$, $a = 1.0\lambda_0$.

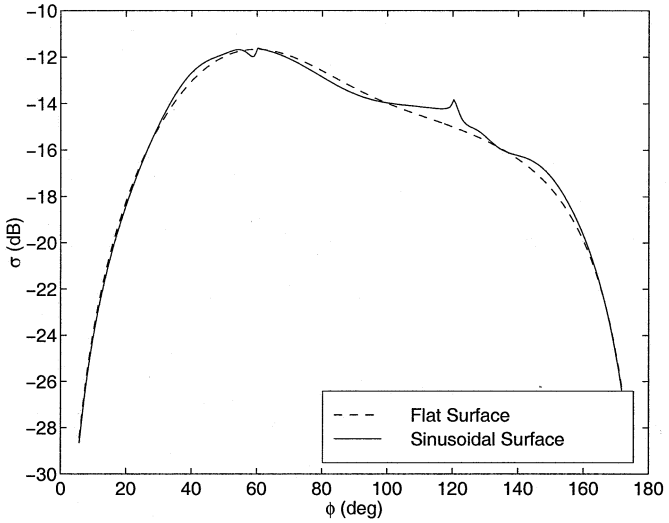

Fig. 8. Effect of sinusoidal surface roughness on the scattering pattern for $\lambda_s = 0.4\lambda_0$, $a = 1.0\lambda_0$.

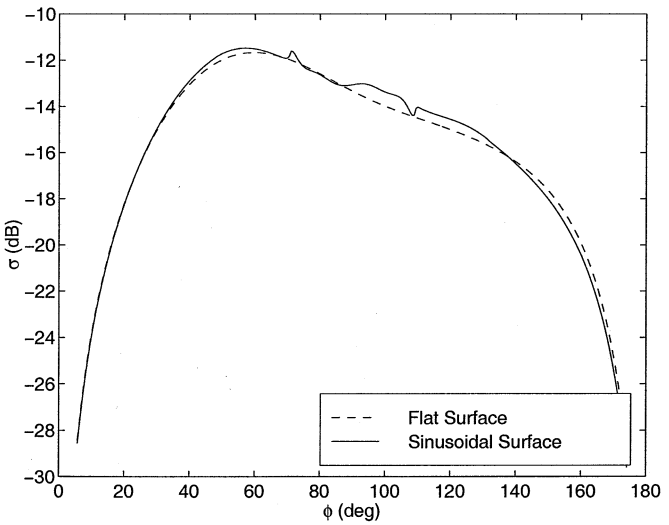

Fig. 9. Effect of sinusoidal surface roughness on the scattering pattern for $\lambda_s = 0.6\lambda_0$, $a = 1.0\lambda_0$.

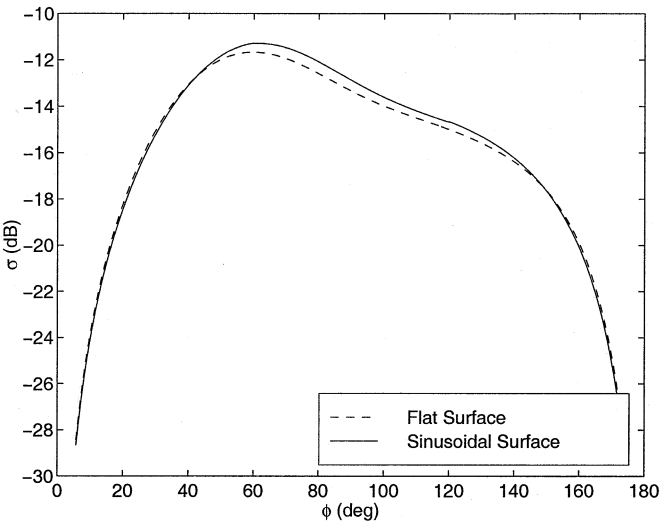

Fig. 10. Effect of sinusoidal surface roughness on the scattering pattern for $\lambda_s = 2.0\lambda_0$, $a = 1.0\lambda_0$.

tion to ask is whether the SPM solution is even valid when the sinusoidal surface has a long period. To address this question, a comparison is made between the SPM solution and the solution obtained from the extended boundary condition (EBC) approach for a sinusoidal surface without a buried object. The EBC solution, outlined in [29], provides coefficients for the discrete angular spectrum of plane waves scattered from the surface and propagating along

$$\mathbf{k}_{jn} = k_{nx}\hat{x} + k_{jny}\hat{y} \tag{29}$$

where

$$k_{nx} = k_x^i + \frac{2\pi n}{\lambda_s} \quad \text{and} \quad k_{jny} = \sqrt{k_j^2 - k_{nx}^2}.$$

The subscript n denotes the nth scattered plane wave and is referred to as the nth Floquet mode. A comparison between the SPM and EBC reflection coefficients for modes in the range,

TABLE I
MAGNITUDE COMPARISON OF FLOQUET MODE REFLECTION COEFFICIENTS FROM A SINUSOIDAL SURFACE, $f(x) = 0.0064\lambda_0 \cos(2\pi/\lambda_s x)$, USING EBC AND SPM. TM CASE WITH $\phi_i = -60^\circ$ AND $\epsilon_1 = 4.0\epsilon_0$

Mode	$\lambda_s = 0.1\lambda_0$		$\lambda_s = 1.0\lambda_0$		$\lambda_s = 10\lambda_0$	
n	EBC	SPM	EBC	SPM	EBC	SPM
-2	2.014e-4	-	2.420e-4	-	2.336e-4	-
-1	2.028e-3	1.990e-3	1.329e-2	1.330e-2	1.295e-2	1.296e-2
0	3.809e-1	3.820e-1	3.816e-1	3.820e-1	3.815e-1	3.820e-1
+1	1.838e-3	1.796e-3	2.152e-2	2.152e-2	1.376e-2	1.377e-2
+2	2.020e-4	-	3.761e-4	-	2.308e-4	-

TABLE II
MAGNITUDE COMPARISON OF FLOQUET MODE REFLECTION COEFFICIENTS FROM A INUSOIDAL SURFACE, $f(x) = 0.0064\lambda_0 \cos(2\pi/\lambda_s x)$, USING EBC AND SPM. TE CASE WITH $\phi_i = -60^\circ$ AND $\epsilon_1 = 4.0\epsilon_0$

Mode	$\lambda_s = 0.1\lambda_0$		$\lambda_s = 1.0\lambda_0$		$\lambda_s = 10\lambda_0$	
n	EBC	SPM	EBC	SPM	EBC	SPM
-2	2.304e-3	-	1.158e-4	-	1.965e-4	-
-1	1.102e-2	1.075e-2	1.700e-2	1.701e-2	1.029e-2	1.030e-2
0	2.820e-1	2.829e-1	2.823e-1	2.829e-1	2.825e-1	2.829-1
+1	1.093e-2	1.075e-2	1.818e-3	1.818e-3	9.442e-3	9.448e-3
+2	2.275e-3	-	1.397e-4	-	1.436e-4	-

$-2 \leq n \leq 2$, are given for the TM and TE cases in Tables I and II, respectively. Since the SPM coefficients are proportional to the Fourier transform of the surface variation function, and the Fourier transform of a sinusoidal function contains Delta functions located at $k_x = \pm 2\pi/\lambda_s$, SPM coefficients for a sinusoidal surface only exist for $n = \pm 1$. It is not necessary for the first-order SPM solution to predict higher order modes because the EBC coefficients for $n = \pm 2$ and higher are seen to be at least an order of magnitude smaller than the $n = \pm 1$ coefficients. The $n = 0$ component is simply the Fresnel reflection coefficient from an unperturbed, flat surface. As seen in the tables, the SPM solution accurately predicts the Floquet mode coefficients for the three dominant modes $(n = 0, \pm 1)$, and the agreement is maintained as the period of the surface variation is increased. Although not shown, the SPM solution for the transmission coeffiecients have similar agreement. These results justify the use of the SPM coefficients in the new solution presented here and validate the results shown in Figs. 3–10.

C. Arbitrary Rough Surface

The final example involves the scattering from a cylinder buried below an arbitrary surface profile. In order to limit the amount of reflected energy from the surface, it is necessary to limit the area illuminated by the incident field. In the rough surface scattering literature, this is usually accomplished by either tapering the incident wave or limiting the extent of the rough surface. For the examples presented here, a Gaussian scaling function, $\exp[-8(x/L)^2]$, is used to taper the generated rough surface, with the constant L providing a measure of the illumination length. Another consideration is the computational complexity of the double integrals, $\Delta I^p_{m,n}$ and ΔI^{tp}_n, for an arbitrary rough surface. These integrals can be made computationally tractable by assuming the rough surface to be periodic, reducing the double integrals to a summation of single integrals weighted by the Fourier series coefficients of the periodic surface. This is a reasonable simplification for a shallow object because the object/rough surface interaction only takes place in a limited area directly above the buried object. Hence, the reduction does not significantly affect the accuracy of the solution provided the period is sufficiently large ($> 10\lambda_0$ and $\gg a$). One should note that the surface is assumed periodic only for the two integrals which account for the object/rough surface interaction. All other integrals are evaluated directly.

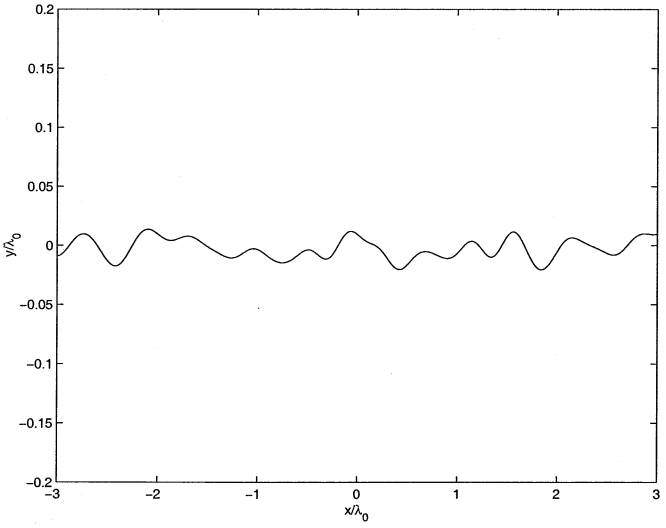

Fig. 11. Single realization of Gaussian rough surface.

Consider the same dielectric cylinder used in Fig. 2 buried at a depth $d = 1.3\lambda_0$ below the rough surface shown in Fig. 11. The surface profile is a sample of a random process with a Gaussian autocorrelation function with correlation length $0.2\lambda_0$, and rms height $0.01\lambda_0$. The permittivity of the ground medium is $\epsilon_1 = (4.0 - j0.01)\epsilon_0$. For a TE incident plane wave at $\phi_i = -60^\circ$, the scattered, reflected, and total far-field patterns are shown in Fig. 12 for an illumination length of $L = 1.25\lambda_0$. When there is no cylinder present, the only scattered field is the initially reflected field, ψ^r_0, from the rough surface. When the cylinder is introduced, the total scattered field is obtained by coherently adding the cylinder component, ψ^s_0, to the initially reflected field. For this particular illumination length and surface roughness, Fig. 12 demonstrates that there is a noticeable increase in the total scattered field when the cylinder is introduced, making object detection possible. An increase in the rms height of the surface roughness will, of course, increase the amount of interference caused by the surface scattering component and make object detection more difficult. Another factor influencing the

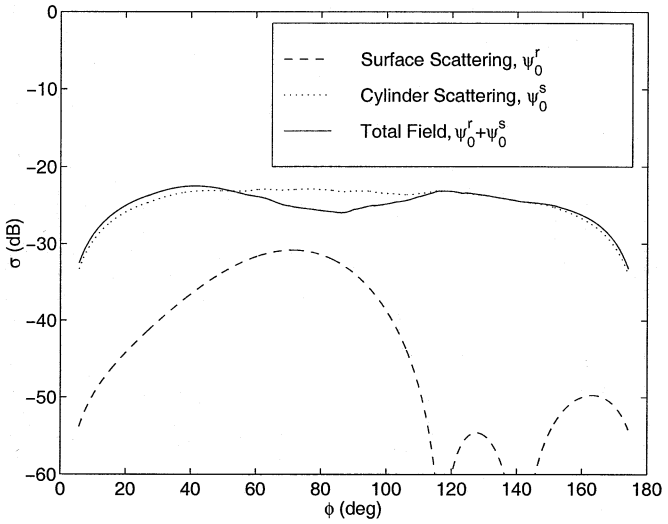

Fig. 12. TE scattering pattern of dielectric cylinder buried at depth, $d = 1.3\lambda_0$, below a rough surface with $L = 1.25\lambda_0$ and $\epsilon_1 = (4.0-j0.01)\epsilon_0$.

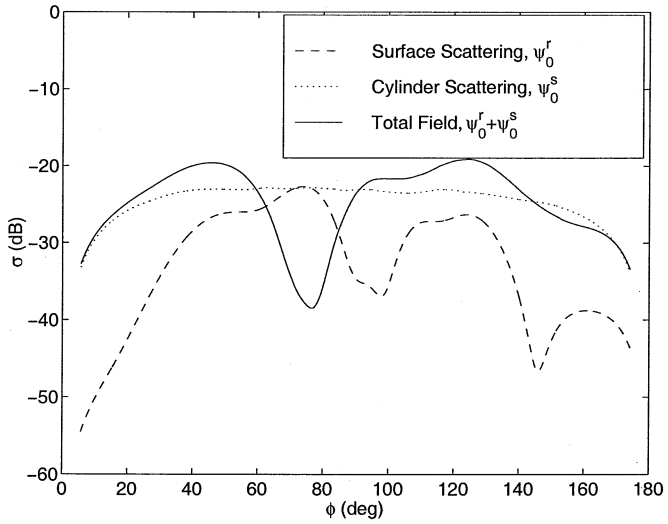

Fig. 13. TE scattering pattern of dielectric cylinder buried at depth, $d = 1.3\lambda_0$, below a rough surface with $L = 5.0\lambda_0$ and $\epsilon_1 = (4.0-j0.01)\epsilon_0$.

visibility of a buried target is the illumination area. An increase in the illumination area will increase the initially reflected field, but will not significantly increase the scattering component from the cylinder. Consequently, for buried-object detection the illuminated area should be as close as possible to the size of the buried objects of interest in order to minimize the interference caused by the rough surface. To illustrate this point, the rough surface from Fig. 11 was simulated with a longer illumination length, $L = 5.0\lambda_0$, and Fig. 13 displays the corresponding scattered fields. As expected, the longer illumination length is seen to increase the interference from the rough surface, making object detection more difficult.

IV. Conclusion

An analytical solution for the electromagnetic scattering from a dielectric cylinder beneath a slightly-rough surface has been presented. This solution accounts for all of the multiple interactions between the rough surface and the buried cylinder and is limited only by the accuracy of the first-order SPM coefficients. The examples illustrate the usefulness of the solution and provide insight into important scattering properties. It was shown that the scattering pattern from a cylinder below a rough surface is only significantly different from the flat-surface case when surface roughness contains a limited range of spatial frequencies. Surface frequencies outside this range do not cause a significant change in the scattering pattern. It was also shown that the area illuminated by the incident wave should be close to the size of the object in order to increase the visibility of the buried object below a rough surface. The solution presented here can be easily extended for other cylindrical buried objects such as dielectric shells or metallic cylinder and may be useful in the development of inversion algorithms for buried targets.

Appendix
Small Perturbation Method Parameters

For the TM case, the unperturbed reflection and transmission coefficients are

$$R_{01}(k_x) = \frac{k_{0y} - k_{1y}}{k_{0y} + k_{1y}} \quad \text{and} \quad R_{10}(k_x) = \frac{k_{1y} - k_{0y}}{k_{1y} + k_{0y}} \tag{30}$$

$$T_{01}(k_x) = \frac{2k_{0y}}{k_{0y} + k_{1y}} \quad \text{and} \quad T_{10}(k_x) = \frac{2k_{1y}}{k_{1y} + k_{0y}} \tag{31}$$

and the TM perturbed components from the SPM are

$$r_{01}(k_x) = \frac{(k_0^2 - k_1^2)2k_{0y}^i}{(k_{0y} + k_{1y})(k_{0y}^i + k_{1y}^i)} jF(k_x - k_x^i) \tag{32}$$

$$r_{10}(k_x, k_x') = \frac{-(k_1^2 - k_0^2)2k_{1y}}{(k_{1y}' + k_{0y}')(k_{1y} + k_{0y})} jF(k_x' - k_x) \tag{33}$$

$$\tau_{01}(k_x) = r_{01}(k_x) \text{ and } \tau_{10}(k_x, k_x') = r_{10}(k_x, k_x'). \tag{34}$$

For the TE case, the unperturbed reflection and transmission coefficients are

$$R_{01}(k_x) = \frac{k_1^2 k_{0y} - k_0^2 k_{1y}}{k_1^2 k_{0y} + k_0^2 k_{1y}} \text{ and}$$

$$R_{10}(k_x) = \frac{k_0^2 k_{1y} - k_1^2 k_{0y}}{k_0^2 k_{1y} + k_1^2 k_{0y}} \tag{35}$$

$$T_{01}(k_x) = \frac{2k_1^2 k_{0y}}{k_1^2 k_{0y} + k_0^2 k_{1y}} \text{ and}$$

$$T_{10}(k_x) = \frac{2k_0^2 k_{1y}}{k_0^2 k_{1y} + k_1^2 k_{0y}} \tag{36}$$

and the TE perturbed components from the SPM are

$$r_{01}(k_x) = \frac{\left(k_0^2 - k_1^2\right)\left(k_x k_x^i k_1^2 - k_{1y} k_{1y}^i k_0^2\right) 2k_{0y}^i}{\left(k_1^2 k_{0y} + k_0^2 k_{1y}\right)\left(k_1^2 k_{0y}^i + k_0^2 k_{1y}^i\right)} \times jF\left(k_x - k_x^i\right) \tag{37}$$

$$r_{10}\left(k_x, k_x'\right) = -\frac{\left(k_1^2 - k_0^2\right)\left(k_x' k_x k_0^2 - k_{0y}' k_{0y} k_1^2\right) 2k_{1y}}{\left(k_0^2 k_{1y}' + k_1^2 k_{0y}'\right)\left(k_0^2 k_{1y} + k_1^2 k_{0y}\right)} \times jF(k_x' - k_x) \tag{38}$$

$$\tau_{01}(k_x) = \frac{\left(k_0^2 - k_1^2\right)\left(k_x k_x^i + k_{0y} k_{1y}^i\right) k_1^2 2k_{0y}^i}{\left(k_1^2 k_{0y} + k_0^2 k_{1y}\right)\left(k_1^2 k_{0y}^i + k_0^2 k_{1y}^i\right)} \times jF(k_x - k_x^i) \tag{39}$$

$$\tau_{10}(k_x, k_x') = -\frac{\left(k_1^2 - k_0^2\right)\left(k_x' k_x + k_{1y}' k_{0y}\right) k_0^2 2k_{1y}}{\left(k_0^2 k_{1y}' + k_1^2 k_{0y}'\right)\left(k_0^2 k_{1y} + k_1^2 k_{0y}\right)} \times jF(k_x' - k_x). \tag{40}$$

REFERENCES

[1] K. Sarabandi and D. E. Lawrence, "Acoustic and electromagnetic wave interaction: Estimation of Doppler spectrum from an acoustically vibrated metallic circular cylinder," IEEE Trans. Antennas Propagat., submitted for publication.

[2] D. E. Lawrence and K. Sarabandi, "Acoustic and electromagnetic wave interaction: Analytical formulation for acousto-electromagnetic scattering behavior of a dielectric cylinder," *IEEE Trans. Antennas Propagat.*, vol. 49, pp. 1382–1392, Oct. 2001.

[3] W. R. Scott Jr, C. T. Schröder, and J. S. Martin, "A hybrid acousto/electromagnetic technique for locating land mines," in *Proc. Int. Geosci. Remote Sensing Symp.*, Seattle, WA, June 1998, pp. 216–218.

[4] B. P. D'Yakonov, "The diffraction of electromagnetic waves by a circular cylinder in a homogeneous half space," *Bull. Acad. Sci. U.S.S.R., Geophys.*, ser. 9, pp. 950–955, 1959.

[5] A. Q. Howard, "The electromagnetic fields of a subterranean cylindrical inhomogeneity excited by a line source," *Geophys.*, vol. 37, no. 6, pp. 975–984, Dec. 1972.

[6] S. O. Ogunade, "Electromagnetic response of an embedded cylinder for line current excitation," *Geophys.*, vol. 46, no. 1, pp. 45–52, Jan. 1981.

[7] S. F. Mahmoud, S. M. Ali, and J. R. Wait, "Electromagnetic scattering from a buried cylindrical inhomogeneity inside a lossy earth," *Radio Sci.*, vol. 16, no. 6, pp. 1285–1298, Nov.–Dec. 1981.

[8] R. Borghi, F. Gori, M. Santarsiero, F. Frezza, and G. Schettini, "Plane-wave scattering by a perfectly conducting circular cylinder near a plane surface: Cylindrical-wave approach," *J. Opt. Soc. Amer.*, vol. 13, no. 3, pp. 483–493, Mar. 1996.

[9] R. Borghi, M. Santarsiero, F. Frezza, and G. Schettini, "Plane-wave scattering by a dielectric cylinder parallel to a general reflecting flat surface," *J. Opt. Soc. Amer.* , vol. 14, no. 7, pp. 1500–1504, July 1997.

[10] R. Borghi, F. Frezza, C. Santini, G. Schettini, and M. Santarsiero, "Numerical study of the reflection of cylindrical waves of arbitrary order by a generic planar interface," *J. Electromagn. Waves and Appl.*, vol. 13, pp. 27–50, 1999.

[11] Q. A. Naqvi and A. A. Rizvi, "Low contrast circular cylinder buried in a grounded dielectric layer," *J. Electromagn. Waves and Appl.*, vol. 12, pp. 1527–1536, 1998.

[12] N. V. Budko and P. M. van den Berg, "Characterization of a two-dimensional subsurface object with an effective scattering model," *IEEE Trans. Geosci. Remote Sensing*, vol. 37, pp. 2585–2596, Sept. 1999.

[13] C. M. Butler, X. B. Xu, and A. W. Glisson, "Current induced on a conducting cylinder located near the planar interface between two semi-infinite halfspaces," *IEEE Trans. Antennas Propagat.*, vol. AP-33, pp. 616–624, June 1985.

[14] X.-B. Xu and C. M. Butler, "Current induced by TE excitation on a conducting cylinder located near the planar interface between two semi-infinite half-spaces," *IEEE Trans. Antennas Propagat.*, vol. AP-34, pp. 880–890, 1986.

[15] P. G. Cottis and J. D. Kanellopoulos, "Scattering of electromagnetic waves from cylindrical inhomogeneities embedded inside a lossy medium with sinusoidal surface," *J. Electromagn. Waves and Appl.*, vol. 6, no. 4, pp. 445–458, 1992.

[16] P. G. Cottis, C. N. Vazouras, C. Kalamatianos, and J. D. Kanellopoulos, "Scattering of TM waves from a cylindrical scatterer buried inside a two-layer lossy ground with sinusoidal surface," *J. Electromagn. Waves Appl.*, vol. 10, pp. 1005–1021, 1996.

[17] K. O'Neill, R. F. Lussky Jr, and K. D. Paulsen, "Scattering from a metallic object embedded near the randomly rough surface of a lossy dielectric," *IEEE Trans. Geosci. Remote Sensing.*, vol. 34, pp. 367–376, Mar. 1996.

[18] L. Tsang, G. Zhang, and K. Pak, "Detection of a buried object under a single random rough surface with angular correlation function in EM wave scattering," *Microwave Opt. Technol. Lett.*, vol. 11, no. 6, pp. 300–304, Apr. 1996.

[19] A. Madrazo and M. Nieto-Vesperinas, "Scattering of light and other electromagnetic waves from a body buried beneath a highly rough random surface," *J. Opt. Soc. Amer.*, vol. 14, no. 8, pp. 1859–1866, Aug. 1997.

[20] J. Ripoll, A. Madrazo, and M. Nieto-Vesperinas, "Scattering of electromagnetic waves from a body over a random rough surface," *Opt. Commun.*, vol. 142, pp. 173–178, Oct. 1997.

[21] A. Madrazo, J. R. Arias-González, and M. Nieto-Vesperinas, "Polarization effects in the scattering of electromagnetic waves by an object beneath a random rough surface," *Opt. Commun.*, vol. 162, pp. 91–98, Apr. 1999.

[22] S. O. Rice, "Reflection of electromagnetic wave by slightly rough surfaces," *Commun. Pure Appl. Math.*, vol. 4, pp. 351–378, 1951.

[23] P. Beckmann and A. Spizzichino, *The Scattering of Electromagnetic Waves from Rough Surfaces*. New York: Pergamon, 1963.

[24] L. Tsang, J. Kong, and R. T. Shin, *Theory of Microwave Remote Sensing*. New York: Wiley, 1985.

[25] R. F. Harrington, *Time-Harmonic Electromagnetic Fields*. New York: McGraw-Hill, 1961.

[26] I. S. Gradshteyn and I. M. Ryshik, *Table of Integrals, Series, and Products*, 5th ed. San Diego, CA: Academic, 1994.

[27] L. B. Felsen and N. Marcuvitz, *Radiation and Scattering of Waves*. Englewood Cliffs, NJ: Prentice-Hall, 1973.

[28] M. F. Chen and A. K. Fung, "A numerical study of the regions of validity of the Kirchhoff and small-perturbation rough surface scattering models," *Radio Sci.*, vol. 23, no. 2, pp. 163–170, 1988.

[29] P. C. Waterman, "Scattering by periodic surfaces," *J. Acoust. Soc. Amer.*, vol. 57, pp. 791–802, 1975.

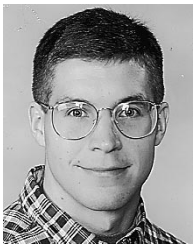

Daniel E. Lawrence (S'96) was born in Silver Spring, MD, on June 8, 1973. He received the B.E.E. and M.S. degrees in electrical engineering from Auburn University, Auburn, AL, in 1996 and 1998, respectively. He is currently working toward the Ph.D. degree at the University of Michigan, Ann Arbor.

From 1997 to 2000, he was a DoD Graduate Research Fellow investigating the use of low-frequency magnetic fields for buried landmine discrimination. He has also performed analytical analysis of acousto-electromagnetic methods applied to buried object detection. His current research interests include microwave and millimeter-wave radar systems, techniques used in buried landmine detection/identification, and the interaction of acoustic and electromagnetic waves.

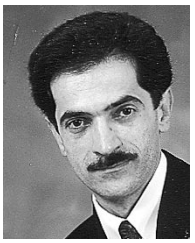

Kamal Sarabandi (S'87–M'90–SM'92–F'00) received the B.S. degree in electrical engineering. from Sharif University of Technology, Tehran, Iran, in 1980. He received the M.S.E. degree in electrical engineering, the M.S. degree in mathematics, and the Ph.D. degree in electrical engineering from The University of Michigan, Ann Arbor, in 1986, 1989, and 1989, respectively.

He is currently the Director of the Radiation Laboratory and Professor in the Department of Electrical Engineering and Computer Science, University of Michigan. He has served as the Principal Investigator on many projects sponsored by NASA, JPL, ARO, ONR, ARL, NSF, DARPA, and numerous industries. He has published many book chapters and more than 90 papers in refereed journals on electromagnetic scattering, random media modeling, wave propagation, antennas, microwave measurement techniques, radar calibration, inverse scattering problems, and microwave sensors. He has also had more than 170 papers and invited presentations in national and international conferences and symposia on similar subjects. His research interests include electromagnetic wave propagation, antennas, and microwave and millimeter-wave radar remote sensing.

Dr. Sarabandi is a member of the IEEE Geoscience and Remote Sensing Society (GRSS) ADCOM, Chairman of the Awards Committee of the IEEE GRSS, and a member of IEEE Technical Activities Board Awards Committee. He is the Associate Editor of the IEEE TRANSACTIONS ON ANTENNAS AND PROPAGATION (AP) and the IEEE SENSORS JOURNAL. He is also a member of Commission F of URSI and of The Electromagnetic Academy. He is listed in *American Men & Women of Science* and *Who's Who in America*. He received the Henry Russel Award from the Regent of The University of Michigan. In 1999, he received a GAAC Distinguished Lecturer Award from the German Federal Ministry for Education, Science, and Technology. He also received a 1996 Teaching Excellence Award from the Electrical Engineering and Computer Science Department of The University of Michigan.